Loss and Efficiency Improvement of EV Traction Drive System by Using SiC in Inverter

Kaninnat Rosdee[1*] Surapong Suwankawin[2]

[1*,2]*Department of Electrical Engineering, Chulalongkorn University, Bangkok, Thailand*

*Corresponding Author. E-mail address: 6370391321@student.chula.ac.th

Received: 26 August 2023; Revised: 3 September 2023; Accepted: 18 October 2023
Published online: 27 December 2023

Abstract

This paper investigates the effectiveness of employing SiC MOSFETs compared to Si-IGBTs in the two-level inverter for the traction motor drives in electric vehicles. The study focuses on the differences in structure and material between SiC MOSFETs and Si-IGBTs by which the conduction and switching losses can be reduced by over 40% and 60%, respectively, when a SiC MOSFET inverter is employed. This advantage enables the SiC MOSFET inverter to drive the traction motor at a higher switching frequency, surpassing traditional Si-IGBT inverters' capabilities. To assess the performance of the systems, simulations are conducted using the PLECS simulation platform. The comparison includes evaluating the traction drive system's efficiency and losses with SiC MOSFET and Si-IGBT inverters on the IPMSM traction motor torque-speed curve; the result shows that the efficiency is improved by over 1% on the entire torque-speed curve. Moreover, the paper also explores the trade-off between the switching frequency and motor harmonic core loss of the motor. This evaluation offers a comprehensive understanding of the interplay between these factors and aids in optimizing the performance of the traction motor system.

***Keywords*:** Conduction loss, Electric vehicles, Harmonic core loss, Switching loss, Wide bandgap

I. INTRODUCTION

Electric vehicles (EVs) are gaining popularity due to their numerous advantages, such as high efficiency, low emissions, and reduced dependency on fossil fuels. However, an EV's performance highly depends on the performance of the power electronics components, particularly the inverter that converts the DC (direct current) from the battery to the AC (Alternating Current) that drives the traction motor.

Power losses in EV drive trains are accounted for 18% of the total electrical power conversion in the system [1]. Two significant losses in the drive trains are 1) the traction motor's power losses and 2) the inverter's power losses. The traction motor's power losses consist of power loss at the conductor (copper loss) and power loss at the iron core (core loss), which are 70% of the drive trains losses. The other 30% of the drive train losses happen in the inverter, which is the loss when the switching devices are conducting the current (conduction loss) and the power loss when the switching devices change state (switching loss).

Power losses in EV drive trains can be reduced by a variety of methods, e.g., motor design [2]–[6], enhancement of motor control methods [3], [5], [7]–[9], development of inverter topologies [10]–[13], improvement of invertzers pulse width modulation (PWM) schemes [14]–[16] and the use of wide band gap (WBG) power switching devices for inverters [17]–[20].

WBG materials are semiconductor materials with a wider energy gap between the valence and conduction band compared to silicon (Si); the widely known WBG materials are, SiC (Silicon Carbide) and GaN (Gallium Nitride). The WBG materials can withstand higher voltage. It also has higher thermal conductivity and saturated electron drift velocity, resulting in better heat dissipation and the ability to operate at higher switching frequencies. Hence, the power-switching devices fabricated from WBG materials are used in the high-performance system. SiC and GaN are both generally fabricated as sub-type of FETs (Field effect transistors). SiC is usually fabricated as MOSFET (Metal-oxide silicon field effect transistor), and GaN is usually fabricated as HEMT (High electron mobility transistor). In [17] presents the application of GaN HEMT devices to two-level inverters for electric vehicles. The drive train efficiency was evaluated with the drive cycle testing. The test results indicated that the drive train efficiency could be increased by over 1% compared with IGBT (Insulated-gate bipolar transistor). However, this work was tested with a low DC bus voltage of 48V, which is too low for the typical electric vehicle application rating. In [18] presents a test of a two-level inverter based on GaN HEMT at 300V DC bus voltage, which is the voltage level for compact EVs. The study shows that inverters can reduce both conduction and switching power losses. The research also investigated the reduction of iron core loss by increasing the switching frequency. The optimum switching frequency must be selected between the switching loss power of the inverter and the power loss at the iron core caused by the switching carrier harmonics. Subsequent research [19] presents a suitable switching frequency control method with a switching frequency map obtained from the test. Article [20] studied the application of a combination of IGBT and GaN HEMT power switches for three-level inverters. It was tested on a system with a DC bus voltage of 800V and various motor driving conditions.

This paper compares the performance and efficiency of two-level three-phase inverters in an EV drive system. Specifically, this study compares the power loss of two-level inverters under different switching frequencies, motor driving conditions, and different types of power switching devices: IGBT and SiC MOSFET. The study is conducted on simulation software that simulates the operation of an EVs motor driving system. The results of this study will provide insight into the suitability of these power-switching devices for EV applications and

help engineers design more efficient and reliable EV drive systems.

The later sections of this paper are organized as follows. Section II describes the losses evaluation of the power switching devices. Motor core loss estimation due to PWM supply is presented in section III. Sections IV and V present the simulation parameters and methods. Simulation results and their analysis are discussed in Section VI. Finally, Section VII provides the study's conclusions.

II. LOSSES MODELLING AND EVALUATION OF THE POWER SWITCHING DEVICES

The power-switching device has two significant losses: conduction loss and switching loss [21]. These losses happen because of the non-ideal switching behaviors of the switching devices, as depicted in Figure 1. Since the loss model of IGBT, MOSFET, and anti-paralleled diode are different. Therefore, the different characteristics are discussed in this section.

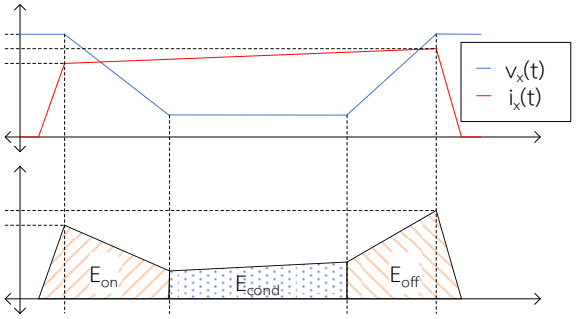

Figure 1: Non-ideal switching behavior of switching devices

A. Conduction Loss Evaluation

The conduction loss of a power-switching device depends on the current it is conducting and the voltage across it during the conduction state. Therefore, the conduction loss is evaluated according to equation (1), where $v_x\ t$, $i_x\ t$ and T is the voltage across the device, the current through the device, and the period of fundamental frequency, respectively. In addition, the subscript x denoted the device types: CE when the device is an IGBT (stands for collector-emitter), DS when the device is a MOSFET (stands for drain-source), or d when the device is a diode.

$$P_{cond} = \frac{1}{T}\int_0^T v_x\ t\ \cdot i_x\ t\ dt \quad (1)$$

The voltage across the device during the conduction state $v_x\ t$ varies depending on the device's current $i_x\ t$ and junction temperature T_j, which differ according to the device's characteristics, as shown in Figures 2 and 3. These data are obtained via the device datasheets.

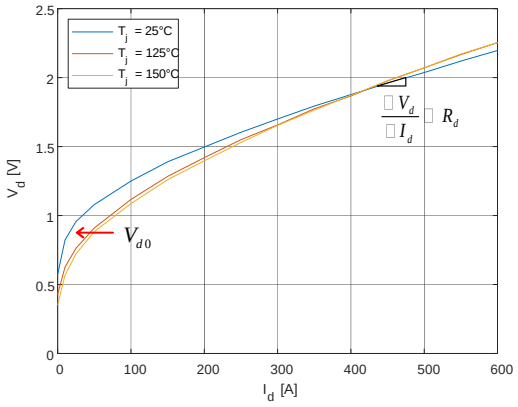

Figure 2: Output characteristic of an IGBT

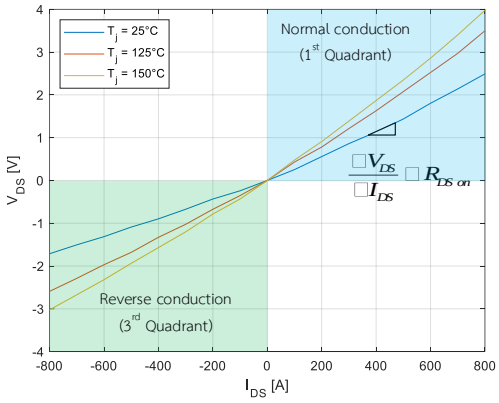

Figure 3: Output characteristic of a MOSFET

Due to the presence of the output bipolar junction transistor, the IGBT features a significantly lower voltage drop when the switch conducts high current. However, as penalties, IGBT has a diode-like voltage drop when it conducts low current. Furthermore, reverse conduction

is impossible because of the additional P-N junction, so the anti-paralleled diode is required, as depicted in Figure 4.

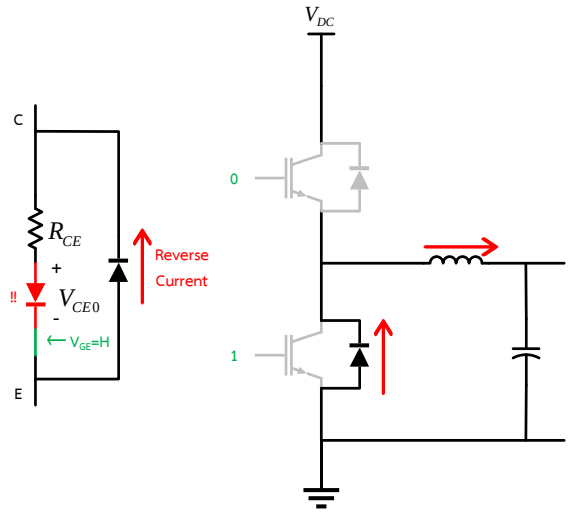

Figure 4: IGBT equivalent circuit and reverse conducting state in a half-bridge circuit

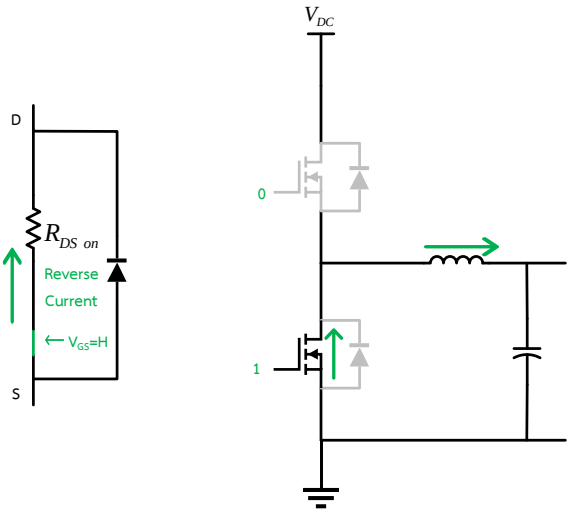

Figure 5: MOSFET equivalent circuit and reverse conducting state in a half-bridge circuit

Therefore, the losses during reverse conduction depend on the anti-paralleled diode's performance and characteristics. Unlike MOSFET, it can be represented as a resistor, so MOSFET can conduct both forward and reverse current, as shown in Figure 5. Moreover, the turn-on state resistance $R_{DS(on)}$ is small in the range of around 100 milliohms, the reverse voltage drop across source and drain $v_{SD}(t)$ will typically not be high enough to forward bias the anti-paralleled diode. Hence, the anti-paralleled diode is required for the conduction during dead time.

B. Switching Loss Evaluation

The switching loss is evaluated from switching energy consisting of turn-on loss and turn-off loss, which the manufacturer provides as a function of the current through the device i_x, the voltage across the device v_x, and the device's junction temperature T_j. Hence, the switching power loss is calculated according to (2)

$$P_{sw} = \frac{1}{T}\int_t^{t+T} \frac{E_{on}(v_x,i_x,T_j)+E_{off}(v_x,i_x,T_j)}{T_s} \cdot dt \quad (2)$$

where T_s is the switching period, and T is the fundamental period, $E_{on}(v_x,i_x,T_j)$ and $E_{off}(v_x,i_x,T_j)$ are the turn-on and turn-off loss at the voltage and current where the state changing occurs. Nevertheless, as shown in Figure 1, for a two-level converter, the voltage at the state-changing points is always equal to the DC bus voltage V_{DC} for either the upper switches (S1, S2, S3) or lower switches (S4, S5, S6). Hence, the switching power loss becomes

$$P_{sw} = \frac{1}{T}\int_t^{t+T} \frac{E_{on}(V_{DC},i_x,T_j)+E_{off}(V_{DC},i_x,T_j)}{T_s} \cdot dt \quad (3)$$

The IGBT and MOSFET have both the turn-on and turn-off loss; however, the turn-on energy loss of a diode or the energy consumed when the diode change state from reverse bias to forward bias is typically low enough to be neglectable. The dominant loss is the turn-off loss, also called reverse recovery loss $E_{rr}(v_x,i_x,T_j)$, which happens because of the charge at the depletion region Q_{rr}. Hence, the switching power loss of a diode is evaluated as follows:

$$P_{rr} = \frac{1}{T}\int_t^{t+T} \frac{E_{rr}(V_{DC},i_x,T_j)}{T_s} \cdot dt \quad (4)$$

III. INTERIOR PERMANENT MAGNET MOTOR CORE LOSS ESTIMATION WITH PWM SUPPLY

The IPMSM's core loss depends on various variables, e.g., the input voltage waveform, structure, motor geometry, stator, and rotor materials. Hence, these details are necessary for motor core loss analysis. By normal means, the famous and accurate method is FEM (Finite element method). However, to simplify the simulation model, this paper used the hysteretic core inductor with a ring shape which is similar to the motor stator shape and the BF (Building Factor) [22]. BF is the ratio between the ring-shaped inductor core loss and actual motor core loss, as shown in Figure 6.

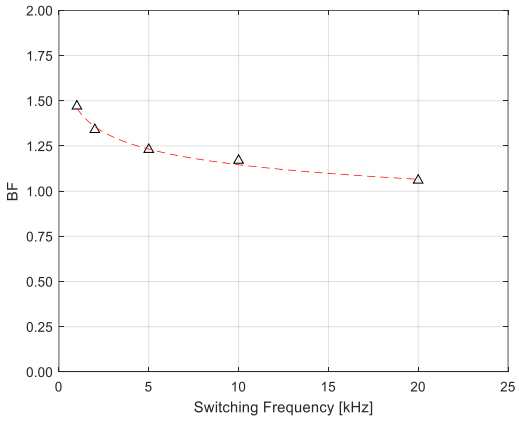

Figure 6: IPMSM building factor vs. supply switching frequency

As widely known, core loss consists of two significant parts; the hysteresis loss P_{hys} and the eddy current loss P_{eddy}, and to model these losses in the inductor core accurately, the non-uniformly discretized model is applied. The advantages of the non-uniformly discretized model are that it includes the skin effect when the core is supplied by a high-frequency supply resulting in an absolute error of less than 5% compared to the actual test results when the frequency of the supply is under 20kHz by implementing only two sections in the non-uniform ladder [23].

The non-uniformly discretized model is constructed by dividing a steel lamination into 2n sub-laminations, where n is the section's number in the non-uniform ladder, and the thickness of the sub-lamination is doubled progressively from the lamination's surface toward the lamination's center. Thus, the sub-lamination thickness and cross-sectional area are calculated as follows:

$$\triangle d_k = \frac{1}{\sum_{j=1}^{n} 2^{(j-k)}} \left(\frac{d}{2}\right) \quad (5)$$

$$A_k = 2 \cdot \triangle d_k \cdot w \quad (6)$$

where d and w are the lamination's thickness and width. The subscript k denotes the kth section in the non-uniform ladder.

The equivalent resistance is used to evaluate the eddy current loss: R_k is the equivalent resistance in the kth section, calculated by the following equation

$$R_k = \frac{2\rho \cdot w}{\triangle d_k \cdot l_e} \quad (7)$$

where r and l_e are the lamination's resistivity and core's magnetic path length.

Finally, the core is constructed by stacking the K layers of steel lamination. Hence, equation (8) and (9) becomes:

$$A_k = 2 \cdot \triangle d_k \cdot w \cdot K \cdot k_s \quad (8)$$

$$R_k = \frac{2\rho \cdot w \cdot K}{\triangle d_k \cdot l_e} \quad (9)$$

where k_s is the lamination's stacking factor.

The hysteresis loss P_{hys} can be calculated according to equation (10).

$$P_{hys} = \frac{1}{T} \int_t^{t+T} H \cdot dB \quad (10)$$

where H, B, T, are the magnetic field strength, magnetic flux density, and fundamental period, respectively. In other words, the hysteresis loss is the area enclosed by the B-H hysteresis loop. Under PWM supply, there are minor B-H hysteresis loops created by the switching pulses in addition to the fundamental B-H hysteresis loop, and these minor loops are causing the additional hysteresis loss, as shown in Figure 7. Therefore, the switching frequency of the PWM supply has a significant impact on these minor hysteresis loops and core loss.

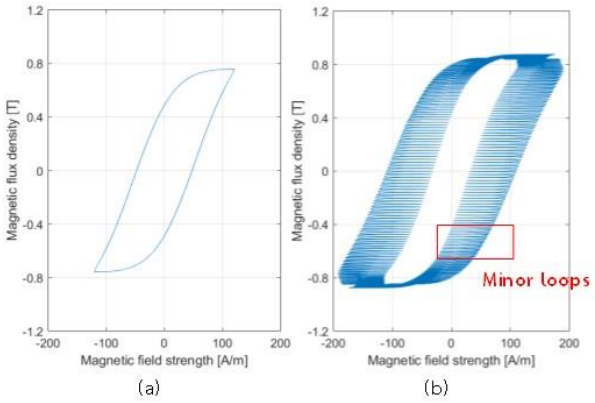

Figure 7: (a) B-H hysteresis loop of 50 Hz sinusoidal supply (b) B-H hysteresis loop of 50 Hz PWM supply (f_s=10kHz)

IV. EVALUATION OF LOSSES REDUCTION OF THE THREE-PHASE INVERTER BY PLECS SIMULATION

This section explains how losses of both the Si-IGBTs and SiC MOSFETs inverters are evaluated using the circuit simulator PLECS.

Figure 8 shows the simulation block diagram for evaluating the inverter loss of an IPMSM (Interior permanent magnet synchronous motor) drive system using PLECS. In the simulation, the three-phase voltages of the IPMSM are supplied by a two-level VSI (Voltage source inverter), which generates the PWM (Pulse width modulation) phase voltages at the switching frequency f_s. The PWM signals are calculated using the 3-arms carrier-based SVPWM (Space vector PWM) technique. For the motor control algorithm, the FOC (Field oriented control) with MTPA scheme (Maximum torque per ampere) and VCLMT scheme (Voltage-current limited maximum torque) are used in the inner control loop. MTPA calculates d-q axis currents that minimize the copper loss in the constant torque region, and VCLMT calculates the d-q axis current in the field weakening region. The outer control loop uses a PI controller as the motor speed regulator.

In PLECS, the device loss data are obtained via datasheets and experimental results as reference data, and these device loss data $E_{on}^{ref}\left(V_{x\_ref}, I_{x\_ref}, T_{j\_ref}\right)$, $E_{off}^{ref}\left(V_{x\_ref}, I_{x\_ref}, T_{j\_ref}\right)$, $E_{rr}^{ref}\left(V_{x\_ref}, I_{x\_ref}, T_{j\_ref}\right)$, $v_{CE}^{ref}(t)$, $v_{DS}^{ref}(t)$ and $v_{d}^{ref}(t)$ are defined as Look-up tables (LUTs). So, when the operating points of the devices are not on the tables, PLECS performs the linear inter/extrapolation. From these device loss data, conduction and switching losses can be evaluated by loss equations in section II.

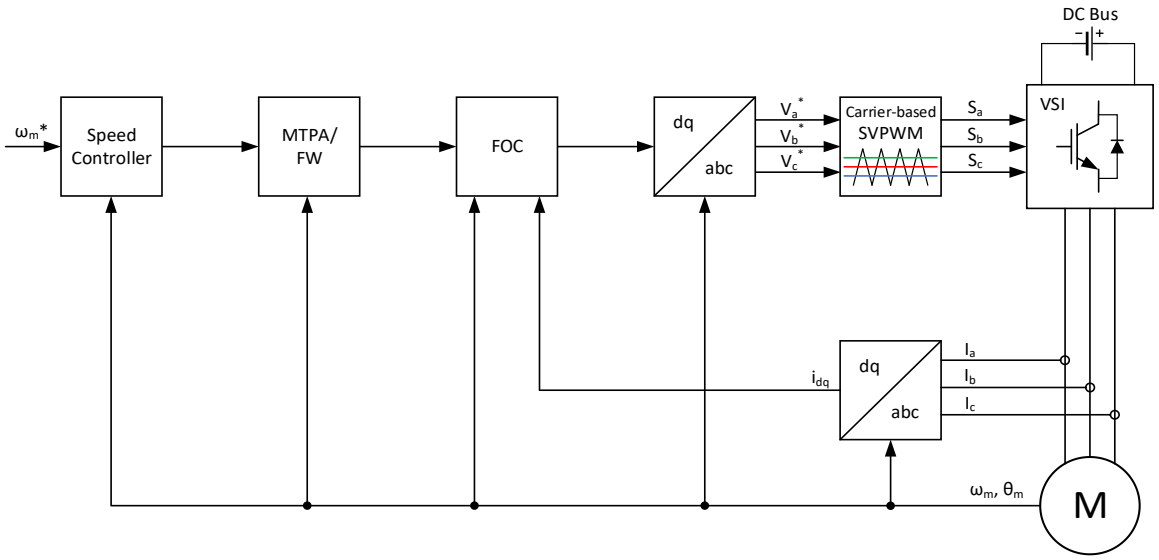

Figure 8: PLECS simulation block diagram

These simulations in PLECS carry out loss evaluations with LUTs; therefore, they can simplify complex parameter identification and loss estimations of power-switching devices. Furthermore, the junction temperature T_j is fixed in the simulations to simplify and reduce simulation time—the following parameters in Table 1, 2, and 3 are used to simulate the traction drive system.

Table 1: Switching device specifications

Classification	Product name	Ratings
SiC MOSFET	FS03MR12A6MA1B	1200V/400A
Si IGBT	FS380R12A6T4B	1200V/380A

Table 2: Simulation setting for losses evaluation

Parameter	Symbol	Value
DC bus voltage	V_{DC}	800V
Switching frequency	f_s	10 kHz, 20 kHz
Dead time	t_{dead}	1.0 μs (IGBT) 0.5 μs (SiC MOSFET)
Junction Temp.	T_j	125°C

Table 3: IPMSM Parameters

Parameter	Symbol	Value
Power Rating	P_{rated}	165 kW
Pole Pairs	p	3
Stator Resistance	R_s	28 mΩ
d-axis Inductance	L_d	0.41 mH
q-axis Inductance	L_q	0.725 mH
Permanent magnet flux	l_{pm}	0.17 Wb
Rotor Inertia	J_r	0.4 kgm^2

V. EVALUATION OF CORE LOSS REDUCTION OF THE IPMSM BY PLECS SIMULATION

The IPMSM core loss is evaluated based on the ring core analogy, as mentioned in section III. The PLECS magnetic domain, which simulates the magnetic circuit based on the permeance-capacitance analogy approach, is used to simulate the losses in the ring core inductor, and the ring core model is based on the non-uniformly discretized model with two sections in the non-uniform ladder. Figure 9 and Table 4 show the non-uniform ladder model and the ring core material and geometry, respectively.

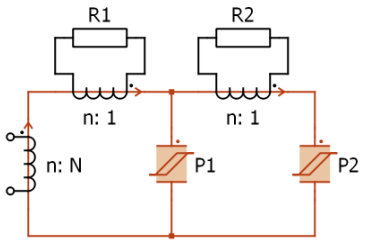

Figure 9: Per phase non-uniformly discretized model in PLECS

Table 4: Ring core material and geometry

Parameter	Symbol	Value
Steel lamination	-	35H300
Height	h	70 mm.
Outer diameter	D_{out}	127 mm.
Inner diameter	D_{in}	102 mm.
Magnetic path length	l_e	360 mm.
Turn number	N	283

VI. SIMULATION RESULTS

A. Comparison of Switching and Conduction Losses and Efficiency on the Ipmsm Torque-Speed Curve

Figures 10 and 11 show each inverter's conduction loss and switching loss at a rotor speed of 5000 r/min (80% of the rated speed). SiC MOSFET inverter can reduce the conduction loss by 40% and 69% at load torque $T_L =$ 225 and 75 Nm at the same carrier frequency and because of the reverse conduction capability; therefore, conduction loss in the anti-paralleled diodes is reduced by over 85%. Also, the SiC MOSFET inverter can decrease the switching loss drastically; as shown in Figure 11, the switching loss of the SiC MOSFET inverter was reduced by 62% at $T_L =$ 225 Nm and 71% at $T_L =$ 75 Nm at the same switching frequency. Even when the SiC MOSFET inverter operates at the 20kHz switching frequency, the switching loss is still lower than the Si-IGBT inverter; hence, the SiC MOSFET inverter is capable of operating

at the double switching frequency and still achieves better efficiency compared to the Si-IGBT inverter. For conduction loss, it does not increase much because the load current is not changed. Nevertheless, the conduction loss of anti-paralleled diodes is doubled because when the switching frequency doubles, it also doubles the conduction time of the diodes since the dead time counts per fundamental period increased. Furthermore, as the dead time increases, the conduction time of the SiC MOSFET decreases; thus, the conduction loss is reduced slightly.

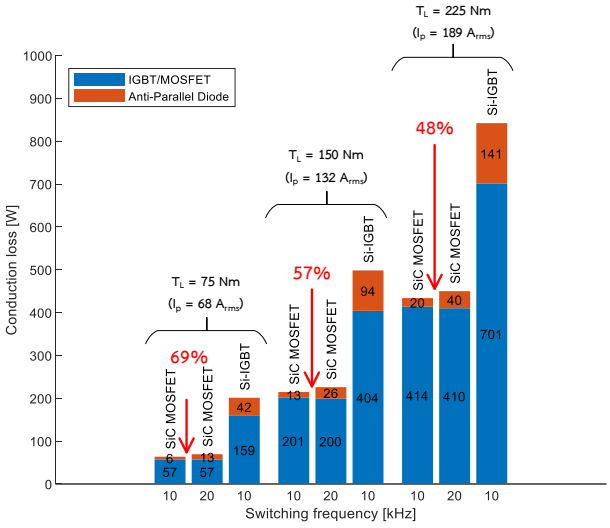

Figure 10: Comparison of conduction loss at w_m = 5000 r/min

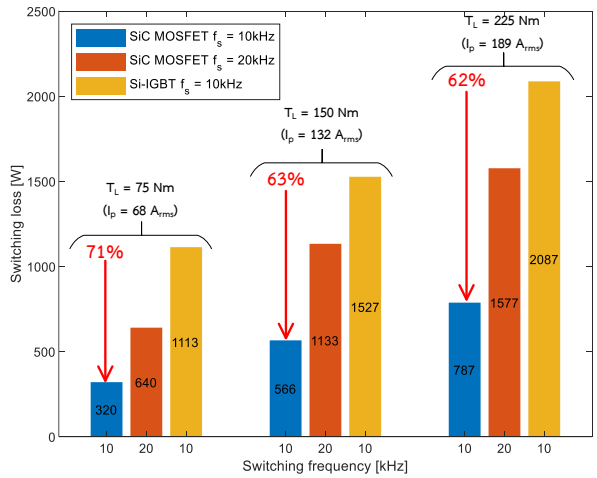

Figure 11: Comparison of switching loss at w_m = 5000 r/min

Si-IGBT and SiC MOSFET inverter efficiency maps on the motor torque-speed curve are shown in Figures 12 and 13. The efficiency improvement is presented in Figure 14. The SiC MOSFET inverter can achieve over 99% efficiency and get over 1% better than the Si-IGBT in a wide area on the torque-speed curve, specifically the high-torque high-speed area. On the other hand, the Si-IGBT can achieve around 98%. Furthermore, in the low-load torque in the field-weakening region near the rated speed (6300 r/min), the efficiency improves by over 20% and slowly decreases. Because, in this region, the inverter must feed the d-axis current continuously to weaken the magnetic flux linkage, which induces the back EMF (Electromotive force). Hence there is always conduction loss occurs. For example, when the motor runs at a speed of 7000 r/min, the d-axis current of around 153A_p must be injected. The voltage across Si-IGBT is around 1.5V_p; conversely, the voltage across SiC MOSFET is only 0.62V_p. As described in Section II, the big difference in voltage drop is the effect of the diode-like voltage drop when Si-IGBT conducts low current. Hence, the conduction loss played a significant part in the efficiency improvement of the FW region's low-torque area. And then, the d-axis current increases with the increasing rotor speed to counteract the back EMF, which reduces the effect of the diode-like voltage drop; therefore, the efficiency improvement slowly decreases.

B. Motor Core Loss Reduction by Increasing the Switching Frequency of the Inverter

As mentioned in the previous section, utilizing the SiC MOSFET allows the inverter to operate at a higher switching frequency without significantly increasing inverter conduction and switching loss. Furthermore, increasing the switching frequency improves motor efficiency because the harmonic core loss of the motor decreases at a higher switching frequency.

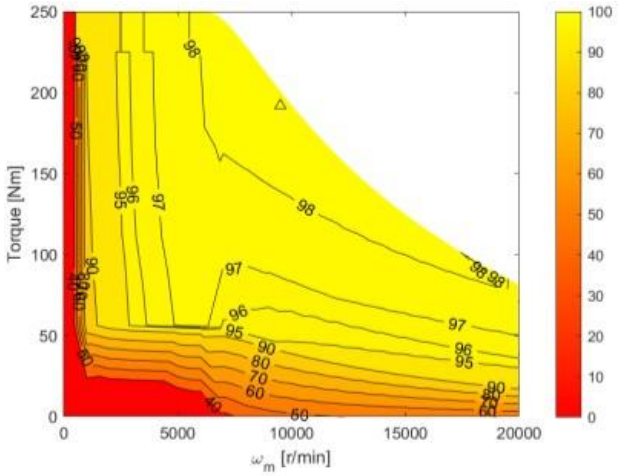

Figure 12: Two-level Si-IGBT inverter efficiency map

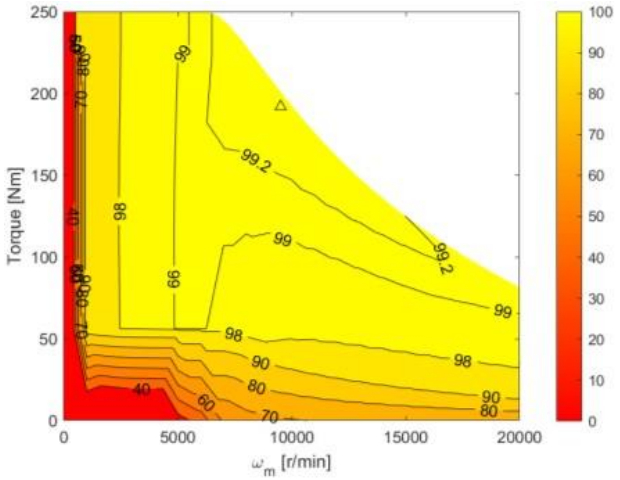

Figure 13: Two-level SiC MOSFET inverter efficiency map

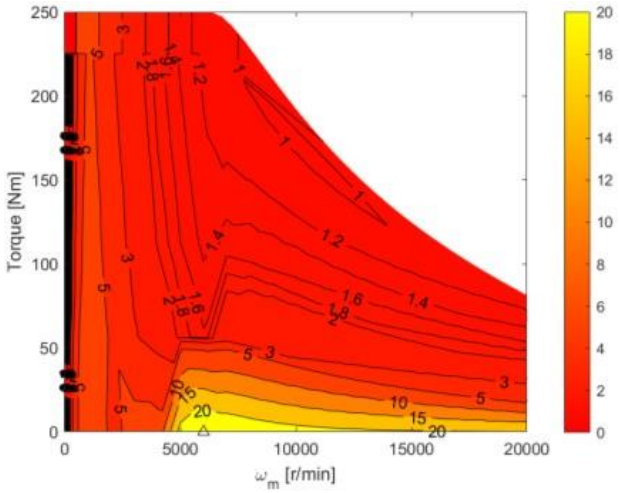

Figure 14: Difference in inverter efficiency

Figure 15 shows the relative core loss reduction of the inverter-fed iron core at switching frequencies of 10 kHz vs. 20 kHz.

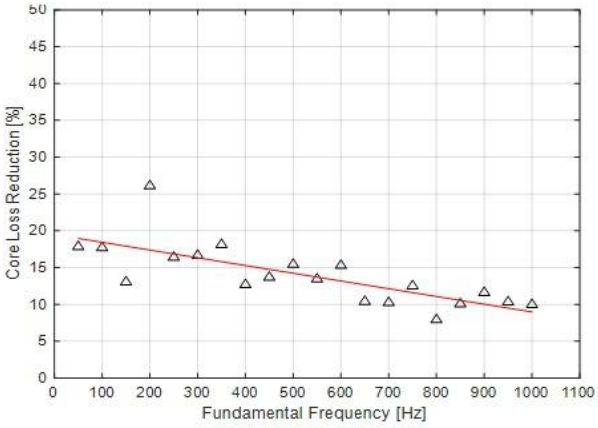

Figure 15: Relative core loss reduction of 10 kHz vs. 20 kHz

Core loss is reduced by up to 20% in the low-speed region and around 10% in the high-speed region. However, the overall efficiency of the drive train may not increase because the increases in the switching frequency mean increases in switching loss of the inverter resulting in inverter efficiency decreases. As shown in Figures 16–18, increasing the switching frequency at every motor's operating point is not always beneficial. Hence, optimizing between inverter switching loss and motor core loss will improve the traction drive system's overall efficiency.

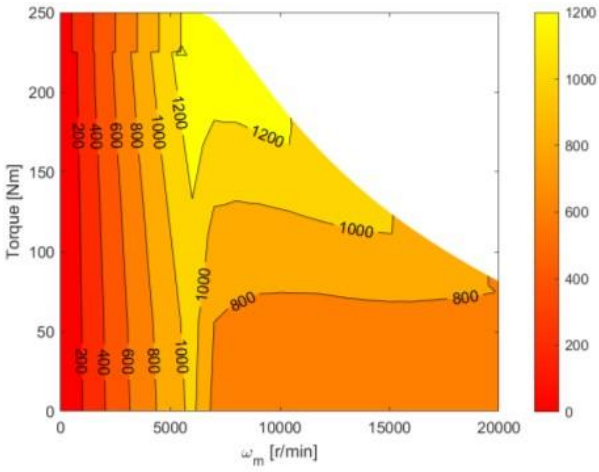

Figure 16: Core loss reduction of 10 kHz vs. 20 kHz (W)

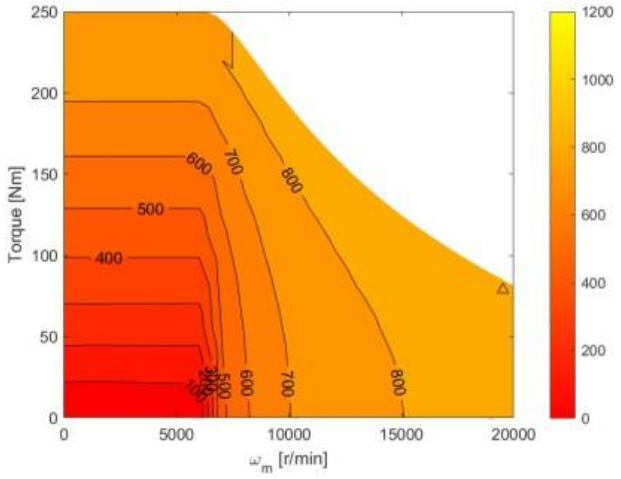

Figure 17: Difference of switching loss 10 kHz vs. 20 kHz (W)

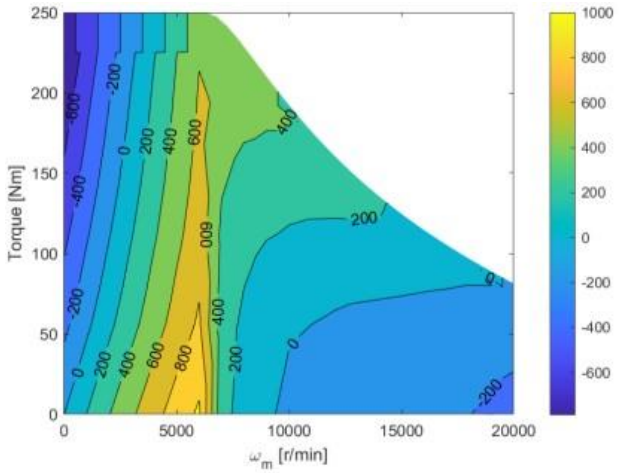

Figure 18: Difference between core loss reduction vs. switching loss increase (W)

VII. CONCLUSION

This paper demonstrates the effectiveness of utilizing a SiC MOSFET inverter—the advantages of employing the SiC MOSFET inverter and IPMSM as the EV drive train was discussed. The SiC MOSFET inverter significantly reduces power losses compared to the Si-IGBT inverter, with over 40% conduction loss reduction and over 60% switching loss reduction. As a result, the inverter and traction drive system efficiency is improved, and core loss reduction of the motor due to the increased switching frequency is evaluated.

REFERENCES

[1] U.S. Department of Energy. “Where the Energy Goes: Electric Cars.” FUELECONOMY.gov. https://www.fueleconomy.gov/feg/atv-ev.shtml (accessed Dec. 1, 2022).

[2] I. Husain *et al.*, “Electric drive technology trends, challenges, and opportunities for future electric vehicles,” *Proc. IEEE*, vol. 109, no. 6, Jun. 2021, pp. 1039–1059.

[3] V. Ruuskanen, J. Nerg, M. Rilla, and J. Pyrhönen, “Iron loss analysis of the permanent-magnet synchronous machine based on finite-element analysis over the electrical vehicle drive cycle,” *IEEE Trans. Ind. Electron.*, vol. 63, no. 7, pp. 4129–4136, Jul. 2016, doi: 10.1109/TIE.2016.2549005.

[4] M. Younkins, P. Carvell, and J. Fuerst, “Dynamic motor drive: Optimizing electric motor controls to improve efficiency,” presented at *42nd Int. Vienna Motor Symp.*, Vienna, Austria, Apr. 29-30, 2021.

[5] L. Shao, A. E. H. Karci, D. Tavernini, A. Sorniotti, and M. Cheng, “Design approaches and control strategies for energy-efficient electric machines for electric vehicles—A review,” *IEEE Access*, vol. 8, pp. 116900–116913, 2020.

[6] Y. Miyama, M. Hazeyama, S. Hanioka, N. Watanabe, A. Daikoku, and M. Inoue, “PWM carrier harmonic iron loss reduction technique of permanent-magnet motors for electric vehicles,” *IEEE Trans. Ind. Appl.*, vol. 52, no. 4, pp. 2865–2871, 2016, doi: 10.1109/TIA.2016.2533598.

[7] O. Wallscheid, M. Meyer, and J. Böcker, “An open-loop operation strategy for induction motors considering iron losses and saturation effects in automotive applications,” in *Proc. IEEE 11th Int. Conf. Power Electron. and Drive Syst.*, Sydney, Australia, 2015, pp. 981–985.

[8] S. Vaez, V. I. John, and M. A. Rahman, “Energy saving vector control strategies for electric vehicle motor drives,” in *Proc. Power Convers. Conf. - PCC '97*, Nagaoka, Japan, Aug. 1997, pp. 13–18.

[9] M. Alnajjar and D. Gerling, “Minimization of energy losses in the traction drive of HEV using optimized adaptive control,” in *Proc. IEEE Veh. Power and Propulsion Conf. (VPPC),* Coimbra, Portugal, 2014, pp. 1–6.

[10] A. Choudhury, P. Pillay, and S. S. Williamson, “Comparative analysis between two-level and three-level DC/AC electric vehicle traction inverters using a novel DC-Link voltage balancing algorithm,” *IEEE J. Emerg. Sel. Topics Power Electron.*, vol. 2, no. 3, pp. 529–540, Sep. 2014.

[11] N. Sorokina *et al.,* "Inverter and battery drive cycle efficiency comparisons of multilevel and two-level traction inverters for battery electric vehicles*,"* in *Proc. IEEE Int. Conf. Environ. and Elect. Eng. and IEEE Ind. & Commercial Power Syst. Eur. (EEEIC / I&CPS Europe)*, Bari, Italy, Nov. 2021, pp. 1–8.

[12] X. Zhang, J. Y. Gauthier, and X. Lin-Shi, "A composite converter with reduced power electronics for electric powertrain applications," in *Proc. IEEE Energy Convers. Congr. and Expo. (ECCE)*, Vancouver, Canada, Oct. 2021, pp. 1468–1475.

[13] E. Libbos, E. Krause, A. Banerjee, and P. T. Krein, "Inverter design considerations for variable-pole induction machines in electric vehicles," *IEEE Trans. Power Electron.*, vol. 37, no. 11, pp. 13554–13565, Nov. 2022.

[14] J.-I. Itoh and T. Ogura, "Evaluation of total loss for an inverter and motor by applying modulation strategies," in *Proc. 14th Int. Power Electron. and Motion Control Conf. EPE-PEMC*, Ohrid, Macedonia, Sep. 2010, pp. S12-21–S12-28, doi: 10.1109/epepemc.2010.5606664.

[15] R. Menon, N. A. Azeez, A. H. Kadam, and S. S. Williamson, "Energy loss analysis of traction inverter drive for different PWM techniques and drive cycles," in *Proc. IEEE Int. Conf. Ind. Electron. Sustain. Energy Syst. (IESES)*, Hamilton, New Zealand, 2018, pp. 201–205.

[16] A. Choudhury, P. Pillay, and S. S. Williamson, "A hybrid PWM-based DC-link voltage balancing algorithm for a three-level NPC DC/AC traction inverter drive," *IEEE J. Emerg. Sel. Topics Power Electron.*, vol. 3, no. 3, pp. 805–816, Sep. 2015, doi: 10.1109/JESTPE.2015.2439296.

[17] K. Kumar and S. B. Santra, "Performance analysis of a three-phase propulsion inverter for electric vehicles using GaN semiconductor devices," *IEEE Trans. Ind. Appl.,* vol. 54, no. 6, pp. 6247–6257, 2018, doi: 10.1109/TIA.2018.2862400.

[18] Y. Nakayama *et al.,* "Efficiency improvement of motor drive system by using a GaN three phase inverter," in *Proc. IEEE Int. Conf. Ind. Technol. (ICIT),* Melbourne, Australia, Feb. 2019, pp. 1599–1604, doi: 10.1109/ICIT.2019.8755018.

[19] K. Ohta *et al.,* "Variable switching frequency control for efficiency improvement of motor drive system by using GaN three phase inverter," in *Proc. IEEE Int. Conf. Ind. Technol. (ICIT),* Buenos Aires, Argentina, Feb. 2020, pp. 119–123, doi: 10.1109/ICIT45562.2020.9067266.

[20] J. Lu, R. Hou, P. Di Maso, and J. Styles, "A GaN/Si hybrid T-type three-level configuration for electric vehicle traction inverter," in *Proc. IEEE 6th Workshop Wide Bandgap Power Devices and Appl. (WiPDA),* Atlanta, GA, USA, 2018, pp. 77–81.

[21] J. Guo, "Modeling and design of inverters using novel power loss calculation and DC-Link current/voltage ripple estimation methods and bus bar analysis," Ph.D. dissertation, Dept. Elect. Comput. Eng., McMaster Univ., Hamilton, Canada, 2017.

[22] N. Denis, S. Odawara, and K. Fujisaki, "Attempt to evaluate the building factor of a stator core in Inverter-Fed permanent magnet synchronous motor," *IEEE Trans. Ind. Electron.*, vol. 64, no. 3, pp. 2424–2432, Mar. 2017.

[23] E. J. Tarasiewicz, A. S. Morched, A. Narang, and E. P. Dick, "Frequency dependent eddy current models for nonlinear iron cores," *IEEE Trans. Power Syst.*, vol. 8, no. 2, pp. 588–597, May 1993.